Available online at www.sciencedirect.com
SCIENCE DIRECT
Solid State Communications 138 (2006) 390–394
solid state communications
www.elsevier.com/locate/ssc

Ordered zinc-vacancy induced $Zn_{0.75}O_x$ nanophase structure

Yong Ding, Rusen Yang, Zhong Lin Wang *

School of Materials Science and Engineering, Georgia Institute of Technology, 771 Ferst Drive, Atlanta, GA 30332-0245, USA

Received 24 February 2006; accepted 24 March 2006 by J.W.P. Hsu
Available online 18 April 2006

Abstract

Using transmission electron microscopy, a new nano-phase structure of $Zn_{0.75}O_x$ induced by Zn-vacancy has been discovered to grow on wurtzite ZnO nanobelts. The superstructure grows epitaxial from the $\{0\bar{1}10\}$ surface of the wurtzite ZnO nanobelts and can be fitted as an orthorhombic structure, with lattice parameters $a'=2a$, $b'\approx\sqrt{3}a$ and $c'=c$, where a and c are the lattice parameters of ZnO. The superstructured phase is resulted from high-density Zn vacancies orderly distributed in the ZnO matrix. This study provides direct observation about the existence of Zn-vacancies in ZnO.

PACS: 61.72.Ff; 61.72.Ji; 68.37.Lp

Keywords: A. ZnO; C. Vacancy; C. Nanobelts; C. Superstructure; E. Transmission electron microscopy

1. Introduction

ZnO is a wide bandgap semiconductor of 3.4 eV [1], which has many applications in optics, optoelectronics, sensors and actuators [2–5]. Recently, with the success in synthesis of one-dimensional nanowires and nanobelts [6], ZnO is becoming an outstanding candidate for nanoscience and nanotechnology [7]. The as-synthesized ZnO nanostructures are usually n-type semiconductor, which has been characterized by scanning surface potential microscopy [8,9]. The excess electrons may be introduced by the presence of hydrogen, Zn interstitials and/or oxygen vacancies [10–12]. Furthermore, the n-type character typically introduces compensating acceptor defects, such as Zn vacancies and oxygen interstitials. Identification and quantification of these point defects are important for their electronic and optoelectronic applications. However, what are the relevant native defects of this oxide is still controversial [13–16]. Many studies have been carried out to define the nature of the defects. The first-principle calculation by Kohan et al. [12] found that the dominant native defects in ZnO are oxygen and zinc vacancies. The positron annihilation spectroscopy study of Tuomisto et al. [17,18] indicated that the Zn vacancies act as the dominant acceptors. There is, however, lacking of a direct proof about the presence of Zn vacancies in ZnO and the distribution of the vacancies in the lattice.

In this work, a new $Zn_{0.75}O_x$ superstructure grown on ZnO one-dimensional nanobelts has been discovered, which is induced by the ordered Zn vacancies. The high-resolution transmission electron microscopy (HRTEM) images recorded from both [0001] and $[0\bar{1}10]$ directions directly show the presence of Zn vacancies in the ZnO lattice. The Zn vacancy-induced superstructure grows epitaxially from the $\{0\bar{1}10\}$ surfaces of the wurtzite structured ZnO nanobelts and can be fitted as an orthorhombic structure, with lattice parameters of $a'=2a$, $b'\approx\sqrt{3}a$ and $c'=c$, where a and c are the lattice parameters of the wurtzite structured ZnO. This study provides a direct observation about the existence of Zn point vacancies in ZnO.

2. Experiment

ZnO nanobelts were synthesized by a solid-vapor deposition process in a horizontal tube furnace [6]. Commercial grade ZnO powders were placed at the center of a single zone tube furnace. A polycrystalline alumina substrate was used for growing the nanostructures. After evacuating for several hours, the temperature of the system was elevated to the synthesis temperature of 1370 °C with Ar carrier gas at the rate of 50 sccm. The pressure was kept at 500 mbar before the temperature reached 800 °C and 200 mbar afterward.

* Corresponding author. Tel./fax: +1 4048948008.
E-mail address: zhong.wang@mse.gatech.edu (Z.L. Wang).

0038-1098/$ - see front matter © 2006 Elsevier Ltd. All rights reserved.
doi:10.1016/j.ssc.2006.03.032

A transmission electron microscopy (TEM) study was carried out at 400 kV using JEM 4000EX and at 200 kV using Hitachi HF2000. The image simulation was done using the Cerius2 software [19].

3. Results and discussion

In a small fraction of the as-synthesized ZnO nanobelts (<5%), TEM imaging and electron diffraction revealed the existence of a superstructure in some local areas of the nanobelts. Fig. 1(a) and (b) show bright-field TEM images of two ZnO nanobelts. Their selected-area electron diffraction (SAED) patterns are displayed in Fig. 1(d) and (e), corresponding, respectively, to the incident electron beam directions of [0001] and $[0\bar{1}10]$ of the wurtzite ZnO. Combining the SAED patterns and TEM images, the nanobelt in Fig. 1(a) grows along $[2\bar{1}\bar{1}0]$ and takes $\pm(0\bar{1}10)$ planes as side surfaces, while the nanobelts in Fig. 1(b) takes $\pm(0\bar{1}10)$ planes as top/bottom surfaces. Besides the diffractions from wurtzite structured ZnO (indexed strong spots), some weak super-lattices are also shown in the SAED patterns, such at $1/2(\bar{2}110)$, $\sim 1/2(0\bar{1}10)$ and $1/4(\bar{2}110)+(0001)=(-1/2\ \ 1/4\ \ 1/4\ \ 1)$. Using small selected-area objective aperture, the super-lattice diffractions in Fig. 1(d) were found to come from the islands at side-surfaces of the nanobelt in Fig. 1(a), as enclosed by the white-rectangle. The inset in Fig. 1(b) is an enlarged dark-field TEM image formed by the super-lattice diffractions in Fig. 1(e), indicates the brighter areas have the superstructure.

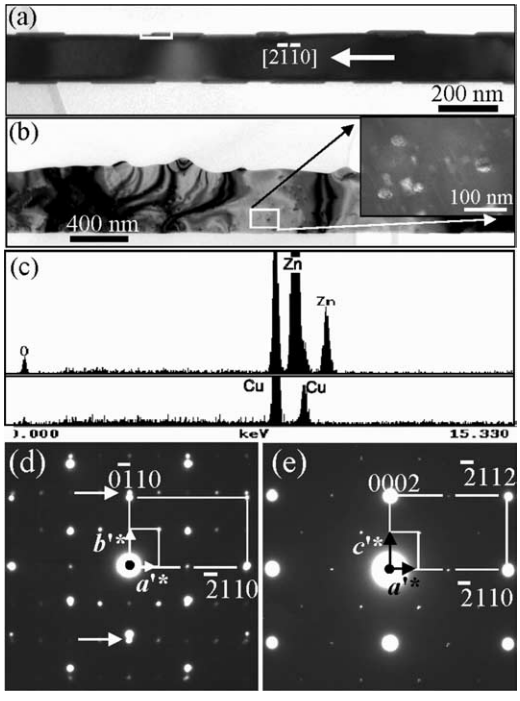

Fig. 1. (a) and (b) Bright-field TEM images of ZnO nanobelts, showing a superstructured phase at the side and top/bottom surfaces of the wurtzite ZnO nanobelts. The inset in (b) is a dark-field TEM image formed by the super-lattice diffractions in Fig. 2(b). The top and bottom EDS spectra in (c) were acquired from the superstructured area (b) and carbon film. (d) and (e) SAED patterns from the nanobelts in (a) and (b), respectively. The weak reflection spots come from the superstructured phase.

Examining the SAED patterns carefully, the superstructure can be fit as an orthorhombic structure. The lattice parameter measured from the SAED patterns in Fig. 1(d) and (e) can be identified as $a'=2a$, $b'\approx\sqrt{3}a$ and $c'=c$, where $a=3.2539$ Å and $c=5.2098$ Å are the lattice parameters of the wurtzite structured ZnO [20]. The unit cell of the superstructure in reciprocal space is emphasized in Fig. 1(d) and (e). The relationship between the superstructure and wurtzite structured ZnO can be described as $(010)'\|(0\bar{1}10)$, $[100]'\|[\bar{2}110]$. The extinction conditions of the superstructure in Fig. 1(d) and (e) can be described as $h00$, $h=2n$ and $h0l$, $h+l=2n$, where n is an integer [21]. The corresponding symmetry operations are 2_1 or 4_2 or 6_3 screw axis and n glide plane. Considering $b'\neq c'$, the space group for the superstructure is likely to be $P2_1nm$ (31) or $P2_1nb$ (33). The model based on HRTEM images to be presented below shows that we cannot identify whether a mirror plane nor a b glide plane perpendicular to c' axis due to the unknown of the precise coordination of oxygen ions. This is limited by HRTEM because of its less sensitivity to light atoms.

Formation of the superstructure corresponds the existence of long-range ordering. Such ordering can be induced by the regular distribution of impurities or Zn, oxygen vacancies or Zn, oxygen interstitials in the matrix. The energy dispersive X-ray spectroscopy (EDS) analysis using a fine electron probe (~3 nm) rules out the possibility of ordered impurities for forming the superstructure (in Fig. 1(c)). The top and bottom spectra in Fig. 1(c) were acquired from the bright-area in the inset of Fig. 1(b) and the supporting carbon film of the TEM grid as a reference, respectively. No other elements are detected in the superstructured phase except oxygen and Zn.

HRTEM images indicate that the ordered Zn vacancies are responsible for the superstructure formation. Fig. 2 is a HRTEM image recorded form the rectangle-enclosed area in Fig. 1(a) with the incident electron beam parallel to [0001]

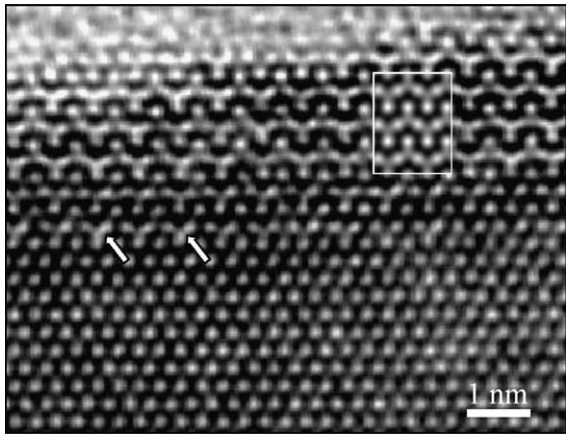

Fig. 2. HRTEM image recorded from the rectangle-enclosed area in Fig. 1(a). The inset is a simulated image based on the model shown in Fig. 3(a). The parameters used for the simulation are: 400 kV, spherical aberration Cs= 0.5 mm, sample thickness as 2.3 nm, defocus as −28.67 nm, objective aperture size 8 nm^{-1}, focus spread 10 nm.

direction of the wurtzite structure. The superstructure has an epitaxial relationship with the wurtzite structured ZnO nanobelt. Image simulations of the perfect wurtzite ZnO crystal with electron beam along [0001] shows that, around the Scherzer defocus, the dark contrast areas adjacent to the bright dots in the HRTEM images correspond to the overlapped Zn and oxygen columns within a large thickness range (1–10 nm). The difference between the superstructured area and the perfect area is the contrast change between those three nearby bright dots, as indicated by the two white arrowheads. Based on the ZnO structural model, we know that the contrast change may be due to the variation of the occupancy of the Zn and/or oxygen atoms in these columns. To match the image contrast, a new structure model is proposed by removing either the Zn or both Zn and oxygen from one projected column and the simulation shows that the contrast change is only sensitive to the missing Zn ions. With a resolution of 0.16 nm, HRTEM image may not be sensitive to the oxygen atoms. Therefore, it is clear that the defect area in the HRTEM image of Fig. 2 is induced by high-density Zn vacancies.

Assuming the existence of Zn vacancies in the defect area and not considering the oxygen vacancies, an atomic model of the superstructure has been built as shown in Fig. 3 based on the HRTEM image displayed in Fig. 2. The model projected along c' axis, corresponding to projecting along [0001] of wurtzite structure, is displayed in Fig. 3(a). Each projected ion column contains alternately stacked Zn and oxygen ions. The zigzag ordered Zn vacancies columns in the $(0\bar{1}10)$ planes form the superstructure, which is consistent with the diffraction pattern shown in Fig. 1(d). The positions of Zn vacancies are marked in yellow. Rotating the model in Fig. 3(a) to project along b' and a' axes, the structures in Fig. 3(b) and (c) are received, respectively. The unit cell of the superstructure is drawn in each of the projected model.

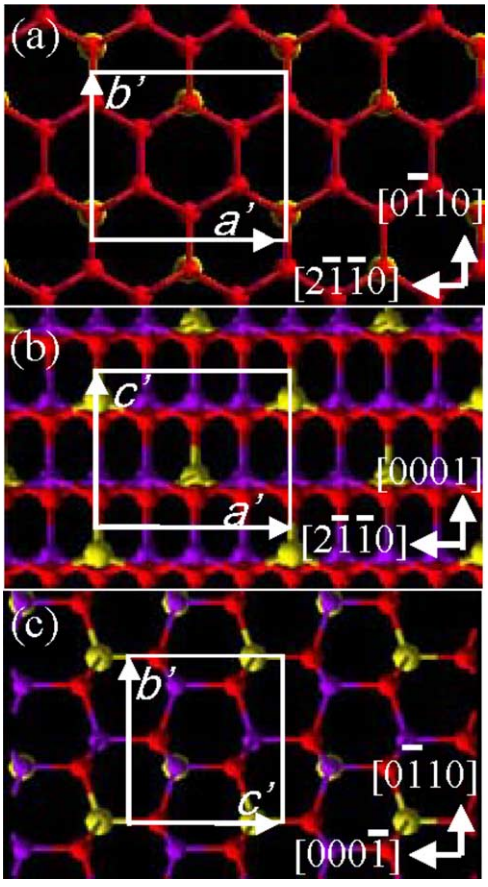

Fig. 3. Atomic model of the superstructure, (a)–(c) projected atomic structures along c', b', and a' axes, respectively. Zn atoms, oxygen atoms and Zn-vacancies are represented by balls in purple, red and yellow colors, respectively (for interpretation of the references to color in this figure legend, the reader is referred to the web version of this article).

The simulated image based on the model in Fig. 3(a) was inserted in Fig. 2, taking the sample thickness as 2.3 nm and defocus as Scherzer defocus (−28.67 nm). The Zn vacancy column shows shallow bright contrast, in good agreement to the image contrast in the superstructured area. This means that the proposed superstructure model is acceptable. On another hand, due to the high density of Zn vacancies accumulated in a set of $(0\bar{1}10)$ planes, the inter-planar distance of the $(0\bar{1}10)$ [or $(010)'$] planes must be compressed in comparison to those in the perfect area. This effect is reflected in the SAED pattern, showing that the $g' = (200)$ diffraction from the superstructure is a little bit longer than the $g = (0\bar{1}10)$ of the perfect crystal (see the parallel arrowheads pointed super-lattice reflections in Fig. 1(d)), and thus the lattice parameter b' is a little shorter than $\sqrt{3}a$. Besides the zigzag-arranged Zn vacancies, there are also some separated Zn vacancies in the atomic columns of ZnO nanobelt matrix as pointed by arrowheads in Fig. 2.

The model in Fig. 3(b) corresponds to the projection along b' axis or $[0\bar{1}10]$ direction, and it can be linked to the nanobelt shown in Fig. 1(b). The superstructure is on the top or bottom large-surfaces of the perfect ZnO nanobelt. In order to further confirm our model, an observation from a different angle is required. The HRTEM images from the nanobelt shown in Fig. 1(b) were recorded, which was oriented along $[0\bar{1}10]$, an angle of 90° from the beam direction for the case in Fig. 2. The image and simulation based on our model shown in Fig. 3(b) have been compared in Fig. 4(a). To include the effect of the substrate effect of the wurtzite ZnO, we carried out the simulation by adding perfect ZnO beneath the model shown in Fig. 3(b). The simulated image is inserted in Fig. 4(a). The sample thickness and defocus used in the simulation are 2.4 nm and Scherzer defocus (−28.67 nm). The thicknesses of the perfect part and superstructured part are taken to be 1.2 nm each. Comparing the experimental image with the simulated one, we know that the dark contrast areas correspond to atom columns. As a reference, an HRTEM recorded from the perfect area (by side of the superstructure area shown in Fig. 4(a)) under the same experimental conditions is shown in Fig. 4(b). The distinct difference between Fig. 4(a) and (b) is due to the existence of the ordered Zn vacancies. The two arrowheads in Fig. 4(a) indicate the positions of the Zn vacancies, which slightly enhance the local intensity.

The HRTEM images and simulation results in Figs. 2 and 4 reveal that the superstructure is formed by ordered Zn vacancies. The extra charge introduced by high-density Zn vacancies in the superstructured area may be neutralized in two

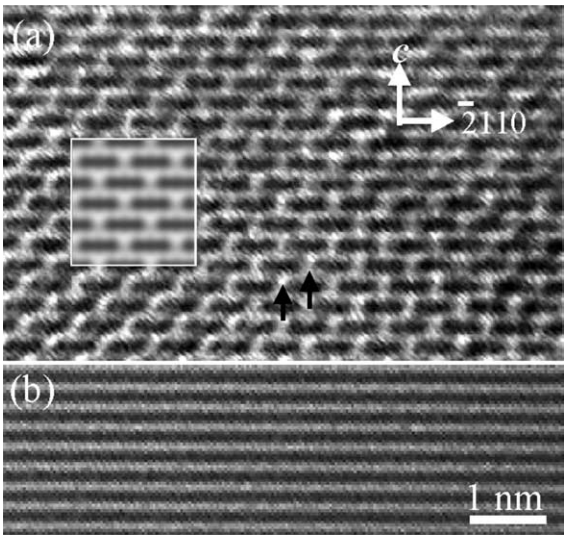

Fig. 4. HRTEM images recorded from the nanobelt shown in Fig. 1(b): (a) from the overlapped area between superstructured phase and the ZnO nanobelt. The inset is a simulated image based on the model presented in Fig. 2(b). The parameters used for the simulation are: 400 kV, spherical aberration Cs = 0.5 mm, objective aperture size 8 nm^{-1}, focus spread 10 nm; (b) from the ZnO substrate, which serves as a reference.

ways. One way is creating compensative oxygen vacancies. The oxygen vacancies may also exist, but our HRTEM is unable to detect oxygen due to its small atomic number. If the superstructured area also suffers from high-density oxygen vacancies, the local mass density (formulated as $Zn_{0.75}O_{0.75}$, just 75% of the density of perfect ZnO crystal) will be too low to make the ion-to-ion bonding stable. Another way is absorbing hydrogen at a local area. There are many studies discussing that hydrogen can serve as relevant shallow donors in ZnO [10,22,23]. It could be possible that the adsorbed hydrogen at the surfaces balance the extra charge of the Zn vacancies, making it possible to form a metastable phase of Zn–O.

The result in Fig. 5 is interesting and may gently support the existence of Zn vacancies in the superstructured phase. The inset SAED pattern in Fig. 5(a) recorded from the whole area indicates the existence of superstructures, which are located at $\pm(0\bar{1}10)$ side surfaces of the nanobelt, as pointed by the arrowheads. Just converging the electron beam of energy 400 keV to illuminate on the nanobelts, the contrast of the superstructure showed obvious change in one minute, and the result is presented in Fig. 5(b). The inserted SAED pattern from the whole area in Fig. 5(b) shows no super-lattice diffractions. It means that the superstructured phase was destroyed by the electron beam irradiation. HRTEM investigation shows that the superstructure areas become amorphous. Thus, the superstructure is more sensitive to high-energy electron beam compared to ZnO nanobelt matrix.

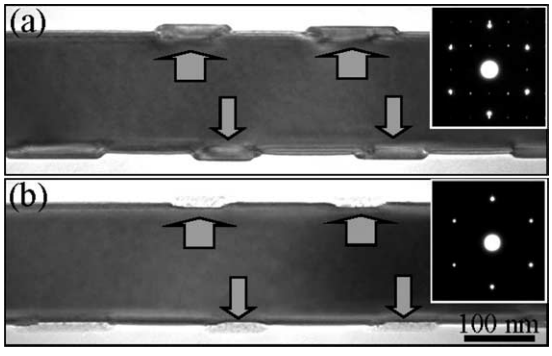

Fig. 5. (a) and (b) Bright-field TEM images and the corresponding SAED patterns of a nanobelt, before and after being irradiated by a converged electron beam at 400 kV, showing the instability of the superstructured phase and its sensitivity to electron beam.

Regardless of whether oxygen vacancies exist or not, our TEM study on the superstructure and the ZnO nanobelt matrix reveals that the Zn vacancies are abound in this material and a new phase of $ZnO_{0.75}O_x$ is formed. This discovery shows that the ZnO nanobelts can have up to 25% of Zn vacancies at least at a local area. Thus, the Zn vacancies should be the dominant acceptors.

4. Conclusion

In summary, using high-resolution transmission electron microscopy, we have identified a new superstructured nanophase in ZnO nanobelts. The superstructure grows epitaxially from the $\{0\bar{1}10\}$ surface planes of the wurtzite structured ZnO nanobelts and can be fitted as an orthorhombic structure, with lattice parameters of $a' = 2a$, $b' \approx \sqrt{3}a$ and $c' = c$. Our results provide a direct observation about the existence of ordered Zn vacancies in ZnO, and has answered a long-standing question about point defects in ZnO. This will be important for guiding the doping and modification of the electronic properties of ZnO.

References

[1] V. Srikant, D.R. Clarke, J. Appl. Phys. 83 (1998) 5447.
[2] K. Vanheusden, W.L. Warren, C.H. Seager, D.R. Tallant, J.A. Voight, B.E. Gnade, J. Appl. Phys. 79 (1996) 7983.
[3] F.-C. Lin, Y. Takao, Y. Shimizu, M. Egashira, J. Am. Ceram. Soc. 78 (1995) 2301.
[4] K.L. Chopra, S. Major, D.K. Pandya, Thin Solid Films 102 (1983) 1.
[5] D.C. Reynolds, D.C. Look, B. Jogai, Solid State Commun. 99 (1996) 873.
[6] Z.W. Pan, Z.R. Dai, Z.L. Wang, Science 291 (2001) 1974.
[7] Z.L. Wang (Ed.), Nanowires and Nanobelts, Kluwer Academic Publisher, New York, 2003.
[8] F.A. Kröger, The Chemistry of Imperfect Crystals, North-holland, Amsterdam, 1974.
[9] Z. Fan, J.G. Lu, Appl. Phys. Lett. 86 (2005) 032111.
[10] D.H. Hoffmann, A. Hofsteatter, F. Leiter, H. Zhou, F. Henecker, B.K. Meyer, S.B. Orlinskii, J. Schmidt, P.G. Baranov, Phys. Rev. Lett. 88 (2002) 045504.
[11] G.D. Mahan, J. Appl. Phys. 54 (1983) 3825.
[12] A.F. Kohan, G. Ceder, D. Morgan, C.V. Van de Walle, Phys. Rev. B 61 (2000) 15019.
[13] P.H. Kasai, Phys. Rev. 130 (1963) 989.
[14] W. Göpel, U. Lampe, Phys. Rev., B 22 (1980) 6447.
[15] D.C. Look, J.W. Hemsky, J.R. Sizelove, Phys. Rev. Lett. 82 (1999) 2552.

[16] S.B. Zhang, S.-h. Wei, A. Zunger, Phys. Rev. B 63 (2001) 075205.
[17] A. Zubiaga, F. Tuomisto, F. Plazaola, K. Saarinen, J.A. Garcia, J.F. Rommeluere, J. Zuñigapérez, V. Muñoz-Sanjosé, Appl. Phys. Lett. 86 (2005) 042103.
[18] F. Tuomisto, V. Ranki, K. Saarinen, D.C. Look, Phys. Rev. Lett. 91 (2003) 205502.
[19] J.M. Cowley, A. Moodie, Acta Cryst. 10 (1957) 609.
[20] JCPDS-80-0075, International Centre for Diffraction Data (1999).
[21] K.H. Kuo, H.Q. Ye, Y.K. Wu, Electron Diffraction Pattern—the Application in Crystallography, Science Press, Beijing, 1983.
[22] C.G. Van De Walls, Phys. Rev. Lett. 85 (2000) 1012.
[23] C.G. Van De Walls, J. Neugebauer, Nature 423 (2003) 626.